JB
Journals.ASM.org

Functional Analysis of the Accessory Protein TapA in *Bacillus subtilis* Amyloid Fiber Assembly

Diego Romero,[a]* Hera Vlamakis,[a] Richard Losick,[b] Roberto Kolter[a]

Department of Microbiology and Immunobiology, Harvard Medical School, Boston, Massachusetts, USA[a]; Department of Molecular and Cellular Biology, Harvard University, Cambridge, Massachusetts, USA[b]

Bacillus subtilis **biofilm formation relies on the assembly of a fibrous scaffold formed by the protein TasA. TasA polymerizes into highly stable fibers with biochemical and morphological features of functional amyloids. Previously, we showed that assembly of TasA fibers requires the auxiliary protein TapA. In this study, we investigated the roles of TapA sequences from the C-terminal and N-terminal ends and TapA cysteine residues in its ability to promote the assembly of TasA amyloid-like fibers. We found that the cysteine residues are not essential for the formation of TasA fibers, as their replacement by alanine residues resulted in only minor defects in biofilm formation. Mutating sequences in the C-terminal half had no effect on biofilm formation. However, we identified a sequence of 8 amino acids in the N terminus that is key for TasA fiber formation. Strains expressing TapA lacking these 8 residues were completely defective in biofilm formation. In addition, this TapA mutant protein exhibited a dominant negative effect on TasA fiber formation. Even in the presence of wild-type TapA, the mutant protein inhibited fiber assembly *in vitro* and delayed biofilm formation *in vivo*. We propose that this 8-residue sequence is crucial for the formation of amyloid-like fibers on the cell surface, perhaps by mediating the interaction between TapA or TapA and TasA molecules.**

Amyloids are a heterogeneous group of proteins initially discovered to be the etiological agents of several human diseases. Proteins in the amyloid conformation are very stable and often form fibrous structures (1, 2). While originally associated only with pathogenesis, it is becoming evident that a large variety of proteins and peptides can take an amyloid form and this is not necessarily related to disease (3). This is particularly apparent in the case of bacterial functional amyloids. For example, functional amyloid-like fibers are found in bacterial species such as *Escherichia coli*, *Bacillus subtilis*, *Pseudomonas* spp., *Streptomyces coelicolor*, and *Staphylococcus aureus*, where they mediate cell-to-cell interactions, attachment to host surfaces, biofilm formation, or raising of aerial structures (4–7).

Interestingly, proteins of different origins and functions with no similarity in amino acid sequence can fold into insoluble amyloid fibers with similar biochemical properties. Further, a common progression of events occurs for all amyloid proteins as they polymerize. The protein is first synthesized as soluble monomers, and then these monomers aggregate through different levels of organization to finally produce organized stable fibers (8, 9). Proteins in different stages of the aggregation process possess different biochemical and morphological features which allow monitoring of polymerization kinetics using colorimetric and microscopic techniques (10).

The curli amyloid fibers in uropathogenic *E. coli* are the best-studied functional amyloids. The products of two distinct operons, *csgBAC* and *csgDEFG*, are dedicated to the formation of curli amyloid fibers in *E. coli* and presumably other curliated Gram-negative bacteria (4, 11). Briefly, curli fibers are composed of two proteins, the major curlin subunit CsgA and the minor subunit CsgB, which nucleates and promotes the polymerization of CsgA outside the cell (12). Both curlin subunits have an amyloid core formed of five imperfect repeats (13), and it is proposed that CsgB provides the template for the correct fold of CsgA from monomers to insoluble aggregates and, eventually, fibers (14, 15). In the Gram-positive bacterium *S. coelicolor*, chaplins are the proteins that polymerize into amyloid fibers (5, 16). Eight distinct chaplins with high levels of similarity in sequence exist (17). All of them have what is known as the chaplin domain, and only the three long chaplins (ChpA, ChpB, and ChpC) have a C-terminal sorting signal to covalently anchor to cell surfaces via sortase activity. It has been proposed that chaplins C, E, and H are indispensable to form the initial chaplin apparatus (18). However, little is known about how the polymerization occurs.

Our work focuses on the soil-dwelling bacterium *B. subtilis*, which produces architecturally complex and ordered communities called biofilms (19). To form a biofilm, *B. subtilis* produces an extracellular matrix mainly composed of an exopolysaccharide and the amyloid-like protein TasA (20, 21), along with the small protein BslA (formerly YuaB) (22–24). As is found in other amyloid proteins, TasA has the propensity to polymerize into fibers enriched in β sheets and highly resistant to degradation or denaturation (9, 21). TasA fibers are used by *B. subtilis* to build a network that connects cells and may organize the rest of the components of the extracellular matrix (21). *In vivo*, the polymerization of TasA into amyloid fibers requires all three members of the *tapA-sipW-tasA* operon (20). SipW is a bifunctional protein that has dedicated signal peptidase activity for processing and secretion of TapA and TasA and also regulates expression of genes

Received 18 November 2013 **Accepted** 29 January 2014
Published ahead of print 31 January 2014
Address correspondence to Roberto Kolter, rkolter@hms.harvard.edu.
* Present address: Diego Romero, Instituto de Hortofruticultura Subtropical y Mediterránea la Mayora (IHSM-UMA-CSIC), Departamento de Microbiología, Facultad de Ciencias, Universidad de Málaga, Málaga, Spain.
Supplemental material for this article may be found at http://dx.doi.org/10.1128/JB.01363-13.

doi:10.1128/JB.01363-13

TABLE 1 Strains used in this study[a]

B. subtilis strain	Genotype	Reference or source
168	Prototroph	19
SSB149	168 (*tapA-sipW-tasA*)::*spc*	45
NCIB 3610	Wild type, undomesticated strain	19
SSB488	*epsA-O*::*tet*	20
FC268	(*tapA-sipW-tasA*)::*spc amyE*::[*tapA*(*13-234*)-*sipW-tasA*] (*cm*)	46
DR9	(*tapA-sipW-tasA*)::*spc amyE*::[*tapA*(*13-234*)-*sipW-tasA*] (*cm*) *lacA*::P_{tapA}-*tapA*	This study
DR10	(*tapA-sipW-tasA*)::*spc amyE*::[*tapA*(*13-234*)-*sipW-tasA*] (*cm*) *lacA*::P_{tapA}-$tapA^{C1,C3,C4/A}$	This study
DR11	(*tapA-sipW-tasA*)::*spc amyE*::[*tapA*(*13-234*)-*sipW-tasA*] (*cm*) *lacA*::P_{tapA}-$tapA^{C2-C5/A}$	This study
DR12	(*tapA-sipW-tasA*)::*spc amyE*::[*tapA*(*13-234*)-*sipW-tasA*] (*cm*) *lacA*::P_{tapA}-$tapA^{C1-C5/A}$	This study
DR13	(*tapA-sipW-tasA*)::*spc amyE*::[*tapA*(*13-234*)-*sipW-tasA*] (*cm*) *epsA-O*::*tet*	This study
DR14	(*tapA-sipW-tasA*)::*spc amyE*::[*tapA*(*13-234*)-*sipW-tasA*] (*cm*) *lacA*::P_{tapA}-$tapA^{C1,C3,C4/A}$ *epsA-O*::*tet*	This study
DR15	(*tapA-sipW-tasA*)::*spc amyE*::[*tapA*(*13-234*)-*sipW-tasA*] (*cm*) *lacA*::P_{tapA}-$tapA^{C2-C5/A}$ *epsA-O*::*tet*	This study
DR16	(*tapA-sipW-tasA*)::*spc amyE*::[*tapA*(*13-234*)-*sipW-tasA*] (*cm*) *lacA*::P_{tapA}-$tapA^{C1-C5/A}$ *epsA-O*::*tet*	This study
DR17	(*tapA-sipW-tasA*)::*spc amyE*::[*tapA*(*13-234*)-*sipW-tasA*] (*cm*) *lacA*::P_{tapA}-$tapA^{\Delta 194-230}$	This study
DR18	(*tapA-sipW-tasA*)::*spc amyE*::[*tapA*(*13-234*)-*sipW-tasA*] (*cm*) *lacA*::P_{tapA}-$tapA^{\Delta 50-57}$	This study
DR19	(*tapA-sipW-tasA*)::*spc amyE*::[*tapA*(*13-234*)-*sipW-tasA*] (*cm*) *lacA*::P_{tapA}-$tapA^{replace}$	This study
DR20	(*tapA-sipW-tasA*)::*spc amyE*::[*tapA*(*13-234*)-*sipW-tasA*] (*cm*) *lacA*::P_{tapA}-$tapA^{amylo}$	This study
DR21	*lacA*::P_{tapA}-$tapA^{\Delta 50-57}$	This study
DR22	*lacA*::P_{tapA}-$tapA^{WT}$	This study

[a] Unless otherwise stated, the strain background is NCIB 3610.

involved in exopolysaccharide production (25–27). TasA is the main component of the fibers, and TapA is a minor component that is copurified in a 1:100 ratio with TasA (28). TapA is required to anchor the TasA fibers to the cell surfaces (21, 28). Furthermore, a null TapA mutant produces thin and disorganized TasA fibers dispersed in the medium and not associated with the cell surface (28). Indeed, TasA appears to be unstable in a *tapA* mutant; very little TasA can be detected, despite similar levels of *tasA* transcription in both the wild type (WT) and the *tapA* mutant (28). *In vitro*, preparations containing 100:1 TasA-TapA mixtures can be stimulated to form fibers in two ways. In solution, fiber formation is observed after a lowering of the pH by the addition of formic acid (29). Fiber formation can be also be triggered by placing the proteins on hydrophobic (but not hydrophilic) surfaces (29).

In this work, we show that TapA contributes to polymerization of TasA into fibers *in vitro*, and we dissect the TapA sequence features that are required for TasA fiber formation. We identified an 8-residue sequence in the N-terminal half of TapA that is crucial for the initiation of TasA polymerization. Deletion of these residues resulted in cells that lacked TasA fibers and were unable to form biofilms. This mutation also resulted in a dominant negative protein, and the mutant protein prevented the activity of wild-type TapA *in vitro* and *in vivo* when both proteins were expressed in the same cells. In addition, five conserved cysteine residues in TapA play a role, albeit a minor one, in the assembly of a robust biofilm.

MATERIALS AND METHODS

Growth media and culture conditions. LB broth consisted of 1% tryptone (Difco), 0.5% yeast extract (Difco), 0.5% NaCl. MSgg broth consisted of 100 mM morpholinepropanesulfonic acid (MOPS; pH 7), 0.5% glycerol, 0.5% glutamate, 5 mM potassium phosphate (pH 7), 50 μg/ml tryptophan, 50 μg/ml phenylalanine, 2 mM $MgCl_2$, 700 μM $CaCl_2$, 50 μM $FeCl_3$, 50 μM $MnCl_2$, 2 μM thiamine, 1 μM $ZnCl_2$ (19). Media were solidified with the addition of 1.5% agar. For colony architecture, 3 μl of starting culture (grown in LB medium with shaking at 37°C overnight) was spotted onto MSgg agar plates and incubated at 30°C for the times indicated below (20). For pellicle formation, 12 μl of a similar starting culture was added to 2 ml or 1 ml of MSgg broth in a 12- or 24-well microtiter dish, respectively, and incubated without agitation at 30°C for the times indicated below.

Final antibiotic concentrations were as follows: for ampicillin, 100 μg/ml; for the macrolide-lincosamide-streptogramin B antibiotics erythromycin and lincomycin, 1 μg/ml and 25 μg/ml, respectively; for spectinomycin, 100 μg/ml; for tetracycline, 10 μg/ml; for chloramphenicol, 5 μg/ml; and for kanamycin, 10 μg/ml.

Strain construction. The strains used and generated in this study are listed in Table 1. Plasmids were constructed and amplified in *E. coli* XL1-Blue (Stratagene) following manufacturer protocols. To construct plasmid pDFR19 (*lacA*::P_{tapA}-*tapA mls*), a 1,250-bp DNA fragment containing the promoter sequence of *tapA* and the open reading frame of the *tapA* gene was amplified using the primers P_{tapA}-F (5′-TGGCGAATTCTCAG AGTTAAATGGTATTGCTTCACT-3′, where the underlining indicates an EcoRI site) and tapA-R (5′-AAAAAAAAAGGATCCATATTACTGAT CAGCTTCATTGCT-3′, where the underlining indicates a BamHI site). The resulting PCR product was digested with the EcoRI and BamHI enzymes and cloned into plasmid pDR183 (30) cut with the same enzymes.

Site-directed mutagenesis and deletion/replacement of *tapA* were performed using pDFR19 as the template and a Stratagene QuikChange II site-directed mutagenesis kit, following the standard protocols described by the manufacturer.

pDFR18 (*lacA*::P_{tapA}-$tapA^{amylo}$ *mls*) was constructed following procedures similar to those described for pDFR19. A DNA fragment containing the P_{tapA} promoter and *tapA* from *Bacillus amyloliquefaciens* ($tapA^{amylo}$) was amplified with the primers $P_{tapA\text{-}Amy}$-*F* (5′-AAAAAAAAACTCGAG CGATCCCACACCTTTTGAATAAATAACGTTTGG-3′, where the underlining indicates an XhoI site) and $tapA_{Amy}$-*R* (5′-AAAAAAAGTCG ACAACAGTTTTACAGGGGGTAAGGCATGTTCCGA-3′, where the underlining indicates a SalI site). The PCR product was digested with the XhoI and SalI enzymes and cloned into pDR183 cut with the same enzymes.

To construct pDFR15 (pET22b-$tapA^{C1-C5/A}$), pDFR16 (pET22b-$tapA^{\Delta 50-57}$), and pDFR17 (pET22b-$tapA^{replace}$), the genes of the different *tapA* alleles without a signal peptide or stop codon were amplified from pDFR11 (pDR183-P_{tapA}-$tapA^{C1-C5/A}$), pDFR13 (pDR183-P_{tapA}-$tapA^{\Delta 50-57}$) or pDFR14 (pDR183-P_{tapA}-$tapA^{replace}$) using the pair of

primers TapAH-F (5′-AAAAAAAAA-CATATGATATGCTTACAATTT TTC-3′, where the underlining indicates an NdeI site) and TapAH-R (5′-AAAAAAAAACTCGAGCTGATCAGCTTCATTGCT-3′, where the underlining indicates an XhoI site) (28). The fragments were digested with the NdeI and XhoI enzymes and cloned into plasmid pET22-b cut with the same enzymes.

To generate strains DR9 to DR12 and DR17 to DR20 {(*tapA-sipW-tasA*)::*spc amyE*::[*tapA*(*13-234*)-*sipW-tasA*] (*cm*) *lacA*::P_{tapA}-*tapA* alleles *mls*, where *tapA*(*13-234*) indicates that residues 13 to 234 of *tapA* are deleted}, the mutant strain lacking the *tapA-sipW-tasA* operon (SSB149) was transformed by natural competence with pDFR19, pDFR9, pDFR10, pDFR11, pDFR12, pDFR13, pDFR14, and pDFR18, respectively, and positive clones were used as donor strains for transferring the constructs into the strain with a *tapA* deletion (FC268) by means of bacteriophage SPP1-mediated generalized transduction (31). To generate strains DR13 to DR16, the *eps* mutation (in which the entire *epsA* to *epsO* operon was replaced by a tetracycline resistance casette, *epsA-O*::*tet*) (20) was transferred to strains DR9 to DR12 by means of SPP1-mediated generalized transduction and selection on tetracycline.

Protein expression and purification. pDFR5 (pET22b-*tapA*), pDFR15 (pET22b-$tapA^{C1\text{-}C5/A}$), pDFR16 (pET22b-$tapA^{\Delta 50\text{-}57}$), and pDFR17 (pET22b-$tapA^{replace}$) were used for the production of the different versions of the His_6-TapA fusion proteins. These plasmids were transformed into competent *E. coli* BL21 cells. Cultures of *E. coli* BL21 cells bearing the different plasmids were grown in 100 ml of LB medium supplemented with ampicillin with shaking at 37°C to an optical density at 600 nm of 0.5. After 3 h of induction in the presence of IPTG (isopropyl-β-D-thiogalactopyranoside; final concentration, 1 mM), cells were harvested by centrifugation and lysed as previously described (28). The pellet was resuspended in 15 ml of lysis buffer consisting of 1× CelLytic B cell lysis reagent (Sigma) diluted in 20 mM Tris, 500 mM NaCl, 20 mM imidazole, and 1 mM phenylmethylsulfonyl fluoride (PMSF) and supplemented with 100 μg ml^{-1} of freshly prepared lysozyme solution. Further disruption and reduction of viscosity were done by sonication.

The different protein samples were mixed with 1.5 ml of nickel chelating resin (G-Bioscience), properly washed and conditioned, and incubated with gentle agitation for 1 h at room temperature. The mixture was successively washed in 20 mM Tris, 500 mM NaCl, 1 mM PMSF buffer containing 20, 40, or 100 mM imidazole. The proteins were finally eluted in the same buffer amended with 500 mM imidazole. Purified proteins were stored at −20° until used.

The TasA-TapA produced by *B. subtilis* was purified as previously described (21). Briefly, cells were grown in MSgg broth at 30°C for 20 h, and after centrifugation, the cell pellet was extracted twice with saline extraction buffer supplemented with a protease inhibitor mixture (cOmplete; Roche). Cell-free supernatant was filtered through a 0.4-mm-pore-size polyethersulfone bottle-top filter. Purified TasA-TapA was stored at −20°C prior to use.

SDS-PAGE and immunoblotting. Proteins were analyzed by SDS-PAGE with 12% polyacrylamide gels using standard protocols. For immunoblot analysis, the proteins were transferred to a polyvinylidene difluoride membrane and hybridized with anti-TapA antibodies at a dilution of 1:7,000 or anti-TasA antibodies at a dilution of 1:20,000 and a secondary anti-rabbit IgG antibody conjugated to horseradish peroxidase (Bio-Rad) at a dilution of 1:20,000. Blots were developed using a Pierce SuperSignal detection system (Pierce, Thermo Scientific). When fractionating samples into medium, cells, and matrix, the protocol used was that described before (20).

Immunocytochemistry, image capture, and analysis. Biofilms harvested at 24 h were resuspended in 1 ml phosphate-buffered saline (PBS) buffer and dispersed by mild sonication. Cells were separated by centrifugation, fixed with a solution of 4% paraformaldehyde for 7 min, washed in PBS, and resuspended in GTE buffer (50 mM glucose, 10 mM EDTA, pH 8, 20 mM Tris-HCl, pH 8) (32). The fixed cells were blocked with 2% bovine serum albumin (BSA)-PBS for 30 min at room temperature. Anti-TapA primary antibody was used at a dilution of 1:50 in 2% BSA-PBS for 1 h at room temperature. Samples were washed 10 times with PBS and exposed to the secondary goat antirabbit antibody conjugated to fluorescein isothiocyanate (FITC) antibody (Invitrogen, Molecular Probes) at a dilution of 1:100 in 2% BSA-PBS for 1 h at room temperature in the dark. Finally, samples were washed 8 times with PBS and resuspended in fresh GTE buffer before visualization.

Fluorescence microscopy images were taken on a Nikon Eclipse TE2000-U microscope equipped with an X-cite 120 illumination system using a Hamamatsu digital camera (model ORCA-ER). The fluorescence signal was detected using the Chroma Technology filter set no. 52017. Image processing was performed using MetaMorph and Photoshop software.

***In vitro* polymerization assay with ThT and fluorescence.** The kinetics of polymerization of TasA in the presence of the different versions of TapA were followed using thioflavin T (ThT) and fluorescence as described previously (21). Briefly, purified TasA was incubated in 10% formic acid for 10 min. The formic acid was evaporated to dryness in a SpeedVac apparatus. The protein was resuspended in buffer (20 mM Tris, 50 mM NaCl, pH 7) or the same buffer containing TapA purified from *E. coli*. The protein mix was added to a ThT solution to achieve a final ThT concentration of 20 μM in a final volume of 200 μl. The final TasA concentration was 2 μg/μl. TapA was added at various molar ratios, as indicated in the text below for each experiment. The fluorescence was measured in a spectrophotometer (Spectra Max M2; Molecular Devices, Sunnyvale, CA) fluorescence plate reader set up at 438 nm of excitation and 495 nm of emission with a 475-nm cutoff at 30°C with shaking. We note that here we used a greater concentration of protein and a longer treatment with formic acid than we used in previous studies, and this led to different kinetics of polymerization of the TasA preparations (21).

RESULTS

TapA enhances polymerization of TasA into fibers *in vitro*. To form a biofilm, *B. subtilis* uses amyloid-like fibers formed by a major component, TasA, and a minor component, TapA (28). To determine how TapA functions in TasA fiber assembly, we first analyzed the proteins using *in vitro* polymerization assays with the amyloid-binding dye thioflavin T (ThT). ThT fluorescence is red shifted when ThT is bound to proteins having β-sheet structures, and therefore, it is used as an indicator for the formation of amyloid-like structures. Our purified matrix protein preparations from wild-type cells contain oligomers that are composed of TasA and TapA at a ratio of about 100:1 (28, 29). When these matrix protein preparations are treated for 10 min with 10% formic acid, evaporated to dryness, and resuspended in 20 mM Tris, 50 mM NaCl, pH 7 buffer, they polymerize into fibers, which bind ThT. The kinetics of this polymerization are shown in Fig. 1 (No addition). When TapA purified from *E. coli* was added to TasA preparations treated at a molar ratio of 1:3 or 1:20 TapA-TasA, the polymerization was accelerated (Fig. 1, +TapA). Interestingly, with the addition of TapA-TasA at a 1:3 ratio, the maximum value of the signal was 3.5-fold higher than the value for the control with no addition, and when TapA was added to TasA at a 1:20 ratio, the maximum intensity was twice that of the TasA sample that had no additional TapA added. In contrast, adding TapA to TasA at a ratio of 1:100 resulted in only slightly enhanced fluorescence throughout the assay. Thus, adding purified TapA at high enough concentrations enhances fiber polymerization. As a control, we assayed the purified TapA preparation alone in the ThT assay and did not observe any fluorescence (Fig. 1, TapA alone).

Analysis of predicted TapA sequences reveals conserved cysteines and two imperfect repeats. Given the importance of TapA in polymerization (Fig. 1) and anchoring of TasA fibers (28), we

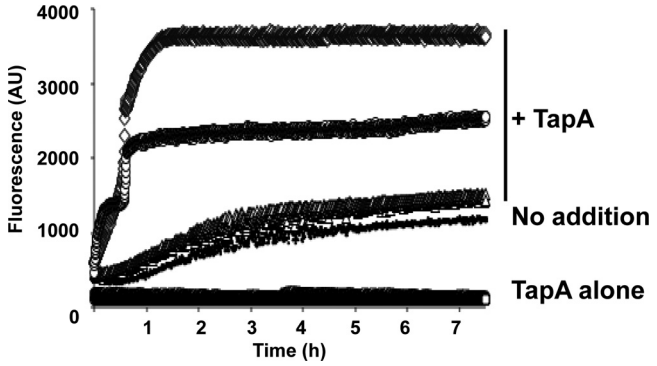

FIG 1 TapA accelerates the polymerization of TasA. Polymerization of purified matrix protein assayed *in vitro* by ThT fluorescence (filled dots; No addition) was the TasA-TapA (100:1) mix purified from wild-type cells. The other curves are for mixtures of the same protein preparation to which TapA was added (+TapA) at the following molar ratios: 1:100 (triangles), 1:20 (circles), or 1:3 (diamonds). TapA alone, TapA with no TasA used as a negative control (squares). The *x* axis is time after ThT addition, and the *y* axis is fluorescence, in arbitrary units (AU).

used bioinformatic analyses to identify potentially important residues or domains that might be involved in the functionality of this protein. Figure 2A shows a general domain structure and the location of the 5 cysteine residues of TapA. The N terminus harbors a signal peptide that allows secretion and processing by the signal peptidase, SipW (26). In addition, there are 5 cysteines that are conserved in alignments of the TapA sequence from *B. subtilis* strain 168 with the TapA sequences from *B. subtilis* subsp. *spizizenii* and *Bacillus amyloliquefaciens* (Fig. 2B). Further analysis using the repeat identification program TRUST (33) showed the presence of two regions, each of which consisted of two highly imperfect repeats: (i) one repeat in the N-terminal half of TapA extending from amino acids 50 to 68 and (ii) one repeat in the C-terminal half composed of residues 194 to 237. Interestingly, the C-terminal region was absent in the more distant relative of *B. subtilis*, *B. amyloliquefaciens* (Fig. 2B).

Role of TapA cysteines in biofilm morphology. A prominent feature of TapA is the presence of five conserved cysteine residues (Fig. 2). Cysteines can have a profound influence on a protein's capacity to form amyloid fibers (17, 34). Thus, we investigated how the TapA cysteine residues might contribute to its functionality. To do so, each cysteine codon was replaced by an alanine codon and the mutated genes (and the wild-type control) were incorporated into the *lacA* locus of a *tapA* mutant. The collection of mutants was then evaluated for pellicle formation in MSgg broth. The replacement of single cysteine residues or combinations of double cysteine mutants did not cause any variation in biofilm morphology compared to that of the wild type. We constructed one mutant lacking 3 cysteines ($tapA^{C1,C3,C4/A}$), one mutant lacking 4 cysteines ($tapA^{C2\text{-}C5/A}$), and a mutant lacking all 5 cysteines ($tapA^{C1\text{-}C5/A}$). These three mutants showed a similar phenotype, with all mutants being partially defective in the formation of biofilms; the result of the mutations in all three mutants was pellicles flatter than those in the wild type (Fig. 3, top row), yet all three mutants formed pellicles slightly more wrinkled than those of the *tapA*-null mutant. A pellicle's architecture relies on two major components: TasA amyloid-like fibers and an exopolysaccharide (20). The presence of the exopolysaccharide might partially mask a decrease in TapA function due to the absence of 3,

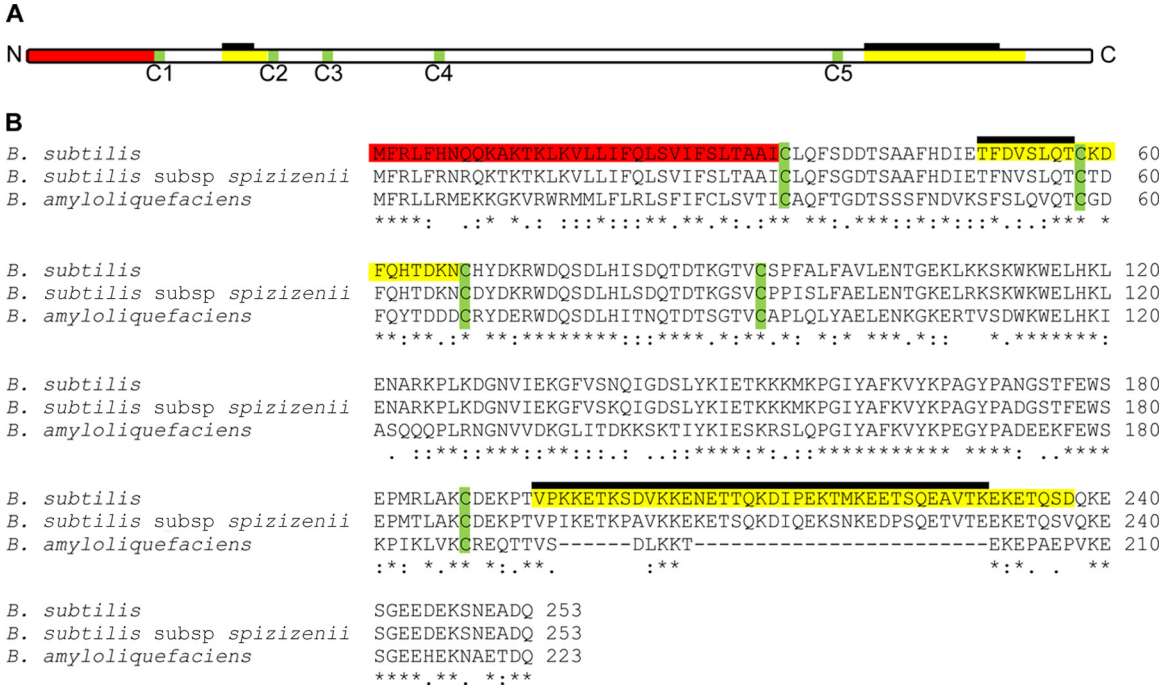

FIG 2 Sequence analysis of TapA. (A) Schematic of the TapA protein sequence. Red, signal sequence; green, five TapA cysteine residues (C1 to C5); yellow, the two imperfect repeats identified by TRUST analysis (33); black lines above the diagram, sequences deleted or replaced in the $TapA^{\Delta 194\text{-}230}$, $TapA^{\Delta 50\text{-}57}$, or $TapA^{replace}$ mutant. (B) Alignment of TapA sequences from closely related *Bacillus* species generated using the Clustal W2 program. Identical residues are marked with asterisks, conserved substitutions are marked with colons, and semiconserved substitutions are marked with periods. The color coding is the same as that described in the legend to panel A.

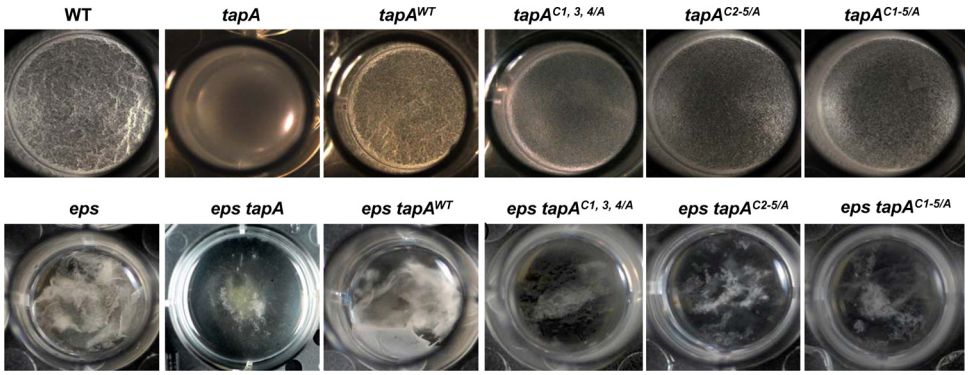

FIG 3 Cysteines contribute to the robustness of biofilms. Top-down views show pellicles of the wild type, a *tapA*-null mutant, and mutant strains DR10 (*tapA*$^{C1,C3,C4/A}$), DR11 (*tapA*$^{C2\text{-}C5/A}$), and DR12 (*tapA*$^{C1\text{-}C5/A}$) (upper row) or the corresponding strains that also harbored a deletion of the *epsA-O* genes (bottom row). Pellicles were grown in MSgg medium for 24 h prior to imaging.

4, or 5 cysteines. To test this, we introduced a deletion of the *epsA-O* operon (*eps*) into the strains whose TapA lacked 3, 4, or 5 cysteines and tested the resulting mutants for pellicle formation (Fig. 3, bottom row). While the *eps* mutant formed very thin broken pellicles, the *eps tapA* double mutant was completely defective in pellicle formation but still grew well, as can be observed by the cells that settled at the bottom of the well. The mutants lacking 3, 4, or 5 cysteines were impaired in pellicle formation and phenocopied an *eps tapA* double mutant lacking the entire *tapA* gene. All of the mutants still produced stable TapA (for example, see Fig. S1 in the supplemental material). Thus, we conclude that the cysteines play a role, albeit a minor one, in TapA function.

Roles of regions containing imperfect amino acid sequence repeats in TapA functionality. Our bioinformatic analysis of TapA revealed two areas containing imperfect amino acid sequence repeats (Fig. 2). The fact that imperfect repeats play an important role in *E. coli* curli assembly (13) led us to assess the role of the TapA repeats in its activity. As an initial step in the functional characterization of these repeats, we constructed mutations that yield altered forms of TapA. To assess the effect of each mutation, we introduced them or the wild-type sequence at the neutral *lacA* locus of a strain that harbored a deletion of *tapA* at its normal chromosomal location and determined their effects on biofilm architecture. The results of these experiments are shown in Fig. 4A, where the panels in the top row show pellicle morphologies, while those in the bottom row show colony morphologies. As controls, the strain with the wild-type *tapA* allele produced pellicles and colonies with robust wrinkling. In contrast, the strain with the *tapA* deletion yielded flat pellicles and colonies.

We first describe the results obtained from investigating the longer repeat located in the C terminus of TapA (residues 194 to 237). In order to determine if this region of TapA is important for its function, we generated a version of the TapA gene lacking a large portion of the repeat by deleting residues 194 to 230 (*tapA*$^{\Delta 194\text{-}230}$). In addition, we made use of a natural variant of this protein by using the *tapA* allele from *B. amyloliquefaciens*, which already lacks this region (*tapA*^{amylo}). In both cases, pellicles and colonies were very similar to those of the wild type (Fig. 4A). Thus, we conclude that the lack of the C-terminal imperfect repeat region does not lead to major phenotypic changes. Our laboratories previously reported that mutations consisting of truncation of the C terminus conferred resistance to the biofilm-inhibiting effects of noncanonical D-amino acids (35). However, recent work indicates that D-amino acids exert their effect indirectly by misincorporation into proteins (36) and that strains with a truncated TapA had likely acquired an unlinked resistance mutation that prevented incorporation of D-amino acids into the protein (S. Leiman and R. Losick, unpublished results).

The results were dramatically different when we deleted part of the imperfect repeat region found on the N-terminal half of TapA (residues 50 to 68). We tested two alleles. In one allele, residues 50 to 57 were lacking (*tapA*$^{\Delta 50\text{-}57}$), and in the other one, those residues were lacking but the residues were replaced by the sequence LGPGIGNG (*tapA*^{replace}). Both alleles yielded flat pellicles and colonies indistinguishable from those produced by the strains harboring the complete deletion of *tapA* (Fig. 4A). The mutant phenotype observed from cells with the *tapA*$^{\Delta 50\text{-}57}$ allele was not due to protein instability because the TapA protein could be detected in the extracellular matrix by immunoblotting with anti-TapA antibody (Fig. 4B). Interestingly, TasA could be detected only in the cell fraction and not in the matrix, indicating that the TapA$^{\Delta 50\text{-}57}$ mutant protein leads to a defect in TasA localization (Fig. 4B). To determine if the mutant TapA$^{\Delta 50\text{-}57}$ protein is properly localized, we performed immunofluorescence microscopy where we visualized TapA using anti-TapA antibodies and a secondary antibody conjugated to FITC. We observed that TapA was indeed localized on the cell surfaces, where it could be seen forming discrete foci in both strains (Fig. 4C). These findings confirmed that the *tapA*$^{\Delta 50\text{-}57}$ allele leads to a loss of function where the TapA protein is still stable and localizes on the cell surface and the matrix. The loss of function appears to be an inability to properly assemble TasA fibers in the extracellular matrix of the biofilm.

Mutant forms of TapA alter polymerization of TasA into amyloid-like fibers *in vitro*. To further investigate how the mutant forms of TapA affected TasA fiber formation, we analyzed the effect of adding purified protein to purified matrix protein (which contains TasA and TapA at a 100:1 ratio) *in vitro*. We used a ThT assay similar to that described in the legend Fig. 1 to study the kinetics of fiber polymerization with no extra addition or in the presence of additional wild-type TapA (+TapA), the mutant form lacking all 5 cysteine residues (+TapA$^{C1\text{-}C5/A}$), or the mutant form with the N-terminal domain deletion (+TapA$^{\Delta 50\text{-}57}$), using thioflavin T fluorescence as a measure of fiber polymerization. The

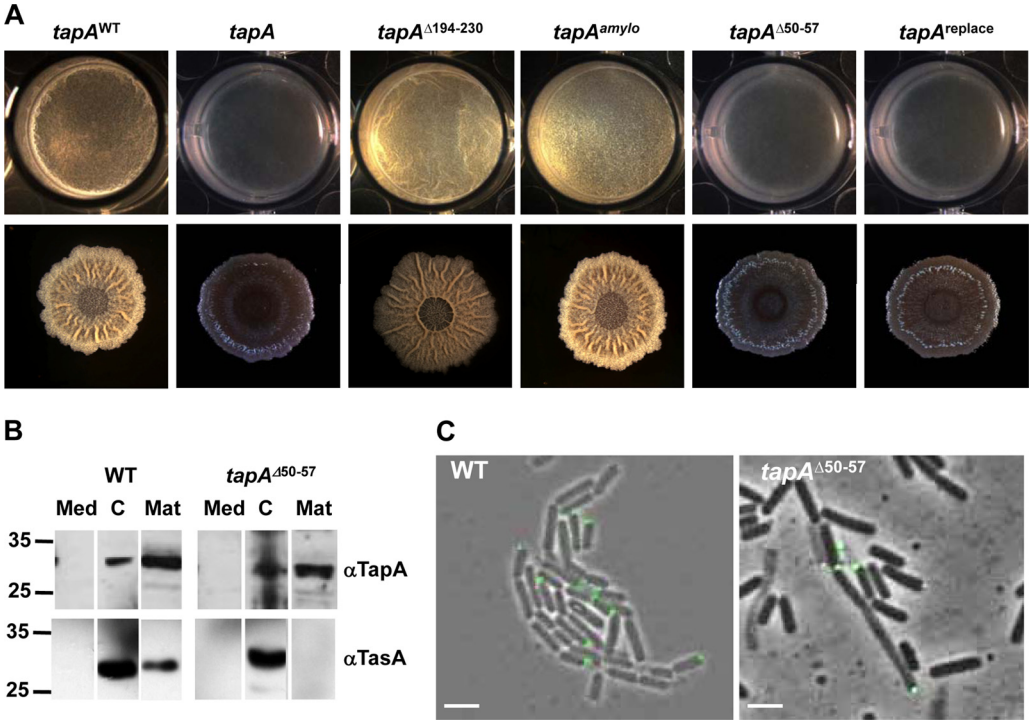

FIG 4 Deletion of TapA residues 50 to 57 inhibits biofilm formation. (A) (Top row) Pellicle formation of *tapA* strains harboring no *tapA* (*tapA*), alleles of wild-type *tapA* from *B. subtilis* ($tapA^{WT}$), *B. amyloliquefaciens* ($tapA^{amylo}$), or *B. subtilis* mutants ($tapA^{\Delta 194-230}$, $tapA^{\Delta 50-57}$), or a replacement of amino acids 50 to 57 ($tapA^{replace}$). (Bottom row) Colony morphology of the same strains from the top row. Pellicles were grown in MSgg broth for 24 h prior to imaging, and colonies were grown in MSgg agar for 72 h prior to imaging. (B) Cells were grown in MSgg medium for 24 h prior to harvesting and separation into medium (Med), cell (C), and extracellular matrix (Mat) fractions. Samples were concentrated and immunoblotted with either anti-TapA (top) or anti-TasA (bottom) antibodies. Numbers on the left are molecular masses (in kilodaltons). (C) Immunocytochemistry with anti-TapA antibody and FITC-conjugated secondary antibody performed on intact cells of wild-type (WT) *tapA* or the $tapA^{\Delta 50-57}$ mutant harvested from pellicles grown in MSgg broth for 24 h. The fluorescence image (green) is overlaid over transmitted light (gray). Bars, 2 μm.

results of these experiments are shown in Fig. 5. The polymerization of TasA with no additional TapA followed typical kinetics, with an initial lag phase, exponential growth, and a slow stabilization of the signal throughout the 7 h of incubation. The addition of wild-type TapA dramatically accelerated the polymerization of TasA and yielded a greater than 3-fold increase in the level of ThT fluorescence. Faster TasA polymerization was also observed in the presence of $TapA^{C1\text{-}C5/A}$, and the final fluorescence was at a level intermediate between that for cells with no additional TapA and that for cells with the addition of wild-type TapA (Fig. 5). This suggests that the cysteine residues play a minor role in the ability of TapA to nucleate the polymerization of TasA. The most surprising result was observed when we added purified TapA lacking amino acids 50 to 57 ($TapA^{\Delta 50-57}$). Not only did this protein fail to enhance the polymerization of fibers, but also it inhibited polymerization completely (Fig. 5). Thus, not only does $TapA^{\Delta 50-57}$ show a loss of function *in vivo*, but also *in vitro* it displays a dominant negative effect on the endogenous wild-type TapA found in our matrix protein preparations.

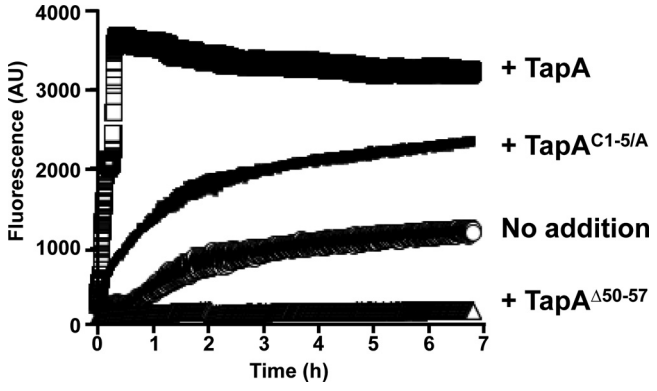

FIG 5 Effect of different TapA proteins on polymerization of TasA. *In vitro* polymerization of TasA-TapA (100:1) (assayed using ThT fluorescence) was performed with no addition or the addition of different TapA proteins to TasA at a 1:3 molar ratio, as indicated. Samples were prepared as described in the legend to Fig. 1.

Deletion of amino acids 50 to 57 of TapA results in a dominant negative protein. Given these *in vitro* results (where $TapA^{\Delta 50-57}$ prevents TasA polymerization), we wanted to test if the $tapA^{\Delta 50-57}$ allele would display a dominant negative phenotype *in vivo*. To this end, we constructed a strain that expressed both wild-type TapA and $TapA^{\Delta 50-57}$. We then analyzed pellicle formation by this strain over a period of 24 h (Fig. 6). While the merodiploid strain harboring a second wild-type allele of *tapA* ($tapA^{WT}$) formed pellicles similar to those of the wild type, the $tapA^{\Delta 50-57}$ allele displayed a dominant negative phenotype in the merodiploid at the earlier times (12 to 18 h). By 24 h, a pellicle formed in the merodiploid strain harboring the $tapA^{\Delta 50-57}$ allele. However, this pellicle was less wrinkled than that formed by the wild-type strain. Thus, it appears that the TapA protein lacking

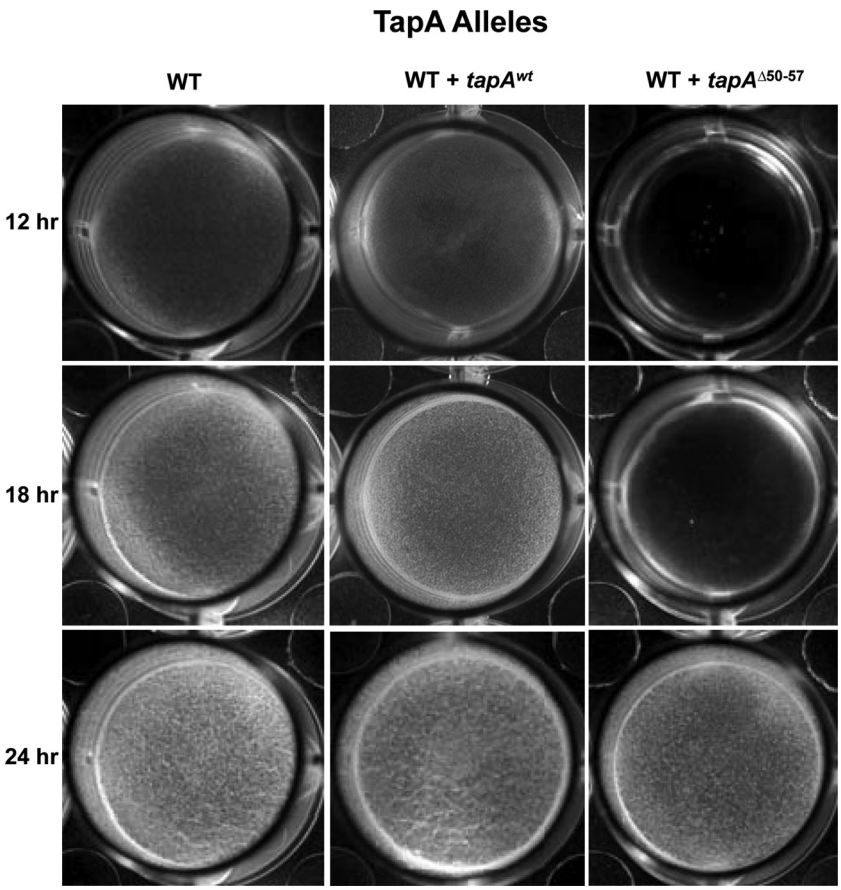

FIG 6 TapA$^{\Delta 50\text{-}57}$ inhibits the functionality of native TapA. A top-down view shows the pellicle formation of the WT strain or merodiploid strains containing the wild-type *tapA* allele (WT), the wild-type *tapA* allele and another copy of wild-type *tapA* (WT + *tapA*^{WT}), or the wild-type allele and the *tapA*$^{\Delta 50\text{-}57}$ allele (WT + *tapA*$^{\Delta 50\text{-}57}$). Pellicles were grown in MSgg medium for the times indicated on the left prior to imaging.

residues 50 to 57 is able to at least partially inhibit the function of wild-type TapA.

DISCUSSION

In bacteria, the formation of amyloid-like fibers is a complex process that requires accessory proteins to control the proper assembly of fibers outside the cell (37). TasA, the major protein found in the matrix of *B. subtilis* biofilms, polymerizes into amyloid-like fibers that are highly resistant to denaturation and degradation (21). Recently, we described TapA, a protein necessary for the anchoring of TasA fibers (28). TapA can be observed as puncta on the cell surface, whereby it presumably aids in the polymerization of TasA into fibers. In the present work, we show that TapA can enhance polymerization of TasA fibers *in vitro*. Furthermore, we identify sequence features that define the functionality of TapA involved in TasA fiber formation. A region of 8 amino acid residues in the N-terminal half of the protein is key for TasA polymerization. We also show that while they are nonessential, the 5 cysteine residues of the protein contribute to the wild-type wrinkling morphology and *in vitro* fiber polymerization.

The role of cysteine residues has also been investigated in *E. coli* curli biosynthesis (38, 39). A cysteine residue is also important in the functionality of CsgG, an oligomeric protein that assembles in pore-like structures facilitating the export of major and minor curlin subunits, CsgA and CsgB. The cysteine is proposed to be the target of CsgC, a periplasmic protein with oxidoreductase activity (39). Pairs of cysteines can oxidize to form disulfide bonds, which contribute to the correct fold and functionality of proteins (40). Importantly, inter- or intramolecular disulfide bonding has been shown to promote or at least stabilize amyloid fibers (41, 42). Furthermore, reducing environments can inhibit or delay amyloidogenesis by blocking intermolecular bonding and thereby preventing fiber growth (34, 43). Even when not totally blocked, amyloid fiber formation can be severely affected under reducing conditions. This is the case for the chaplin amyloid fibers of *Streptomyces coelicolor* (17, 44). Whether reducing conditions will affect TapA function and whether the cysteines that we removed form disulfide bonds remain to be determined.

Analysis of the TapA sequence using the TRUST algorithm (33) predicted two imperfect repeats. One is in the N-terminal half of the protein, and the other is in the C-terminal half of the protein (Fig. 2B, yellow). Mutating the C-terminal repeat did not have any visible effect on TasA fiber formation or on biofilm formation. In contrast, the imperfect repeat found in the N-terminal half of TapA appears to be essential in the formation of TasA fibers. The elimination or replacement of 8 residues of the first repeat abolished TapA activity and even interfered with the functionality of the wild-type TapA. Based on these observations, we propose two possible, not mutually exclusive, functions for this domain. (i) The first function is to participate in the transition of TasA from a

monomeric to a polymeric state. This would be analogous to what is proposed for CsgB-dependent polymerization of CsgA into fibers in *E. coli* (15). (ii) The second function is to mediate the formation of TapA multimers which aid in the polymerization of TasA into fibers on the cell surface. The fact that the TapA$^{\Delta 50\text{-}57}$ mutant displays a dominant negative phenotype with respect to wild-type TapA suggests that TapA must interact with itself to be functional and the mutant TapA inhibits this interaction.

ACKNOWLEDGMENTS

We thank members of the R. Kolter and R. Losick laboratories for helpful discussions and Liraz Chai for valuable comments on the manuscript. We thank Adam Driks (Loyola University Medical Center, Maywood, IL) for kindly providing antibodies against TasA and TapA (formerly known as YqxM). We thank M. Ericsson, L. Trakimas, and E. Benecchi for help and guidance with the electron microscope.

This work was funded by grants to R.K. (GM58213) and R.L. (GM18546). D.R. was funded by a MEC/Fulbright postdoctoral fellowship from the Secretaría General de Estado de Universidades e Investigación del Ministerio de Educación y Ciencia (Spain) and is the recipient of a Ramon y Cajal contract from the Ministerio de Economía y Competitividad (RyC-2011-080605).

REFERENCES

1. **Hardy J, Selkoe DJ.** 2002. The amyloid hypothesis of Alzheimer's disease: progress and problems on the road to therapeutics. Science **297:**353–356. http://dx.doi.org/10.1126/science.1072994.
2. **Fowler DM, Koulov AV, Balch WE, Kelly JW.** 2007. Functional amyloid—from bacteria to humans. Trends Biochem. Sci. **32:**217–224. http://dx.doi.org/10.1016/j.tibs.2007.03.003.
3. **Greenwald J, Riek R.** 2010. Biology of amyloid: structure, function, and regulation. Structure **18:**1244–1260. http://dx.doi.org/10.1016/j.str.2010.08.009.
4. **Chapman MR, Robinson LS, Pinkner JS, Roth R, Heuser J, Hammar M, Normark S, Hultgren SJ.** 2002. Role of *Escherichia coli* curli operons in directing amyloid fiber formation. Science **295:**851–855. http://dx.doi.org/10.1126/science.1067484.
5. **de Jong W, Wosten HA, Dijkhuizen L, Claessen D.** 2009. Attachment of *Streptomyces coelicolor* is mediated by amyloidal fimbriae that are anchored to the cell surface via cellulose. Mol. Microbiol. **73:**1128–1140. http://dx.doi.org/10.1111/j.1365-2958.2009.06838.x.
6. **Dueholm MS, Petersen SV, Sonderkaer M, Larsen P, Christiansen G, Hein KL, Enghild JJ, Nielsen JL, Nielsen KL, Nielsen PH, Otzen DE.** 2010. Functional amyloid in *Pseudomonas*. Mol. Microbiol. **77:**1009–1020. http://dx.doi.org/10.1111/j.1365-2958.2010.07269.x.
7. **Schwartz K, Syed AK, Stephenson RE, Rickard AH, Boles BR.** 2012. Functional amyloids composed of phenol soluble modulins stabilize *Staphylococcus aureus* biofilms. PLoS Pathog. **8:**e1002744. http://dx.doi.org/10.1371/journal.ppat.1002744.
8. **Tjernberg L, Hosia W, Bark N, Thyberg J, Johansson J.** 2002. Charge attraction and beta propensity are necessary for amyloid fibril formation from tetrapeptides. J. Biol. Chem. **277:**43243–43246. http://dx.doi.org/10.1074/jbc.M205570200.
9. **Kajava AV, Baxa U, Steven AC.** 2010. Beta arcades: recurring motifs in naturally occurring and disease-related amyloid fibrils. FASEB J. **24:**1311–1319. http://dx.doi.org/10.1096/fj.09-145979.
10. **Naiki H, Gejyo F.** 1999. Kinetic analysis of amyloid fibril formation. Methods Enzymol. **309:**305–318. http://dx.doi.org/10.1016/S0076-6879(99)09022-9.
11. **Collinson SK, Doig PC, Doran JL, Clouthier S, Trust TJ, Kay WW.** 1993. Thin, aggregative fimbriae mediate binding of *Salmonella enteritidis* to fibronectin. J. Bacteriol. **175:**12-18.
12. **Bian Z, Normark S.** 1997. Nucleator function of CsgB for the assembly of adhesive surface organelles in *Escherichia coli*. EMBO J. **16:**5827–5836. http://dx.doi.org/10.1093/emboj/16.19.5827.
13. **Wang X, Smith DR, Jones JW, Chapman MR.** 2007. *In vitro* polymerization of a functional *Escherichia coli* amyloid protein. J. Biol. Chem. **282:**3713–3719. http://dx.doi.org/10.1074/jbc.M609228200.
14. **Shu Q, Crick SL, Pinkner JS, Ford B, Hultgren SJ, Frieden C.** 2012. The *E. coli* CsgB nucleator of curli assembles to beta-sheet oligomers that alter the CsgA fibrillization mechanism. Proc. Natl. Acad. Sci. U. S. A. **109:**6502–6507. http://dx.doi.org/10.1073/pnas.1204161109.
15. **Hammer ND, Schmidt JC, Chapman MR.** 2007. The curli nucleator protein, CsgB, contains an amyloidogenic domain that directs CsgA polymerization. Proc. Natl. Acad. Sci. U. S. A. **104:**12494–12499. http://dx.doi.org/10.1073/pnas.0703310104.
16. **Claessen D, Rink R, de Jong W, Siebring J, de Vreugd P, Boersma FG, Dijkhuizen L, Wosten HA.** 2003. A novel class of secreted hydrophobic proteins is involved in aerial hyphae formation in *Streptomyces coelicolor* by forming amyloid-like fibrils. Genes Dev. **17:**1714–1726. http://dx.doi.org/10.1101/gad.264303.
17. **Di Berardo C, Capstick DS, Bibb MJ, Findlay KC, Buttner MJ, Elliot MA.** 2008. Function and redundancy of the chaplin cell surface proteins in aerial hypha formation, rodlet assembly, and viability in *Streptomyces coelicolor*. J. Bacteriol. **190:**5879–5889. http://dx.doi.org/10.1128/JB.00685-08.
18. **Duong A, Capstick DS, Di Berardo C, Findlay KC, Hesketh A, Hong HJ, Elliot MA.** 2012. Aerial development in *Streptomyces coelicolor* requires sortase activity. Mol. Microbiol. **83:**992–1005. http://dx.doi.org/10.1111/j.1365-2958.2012.07983.x.
19. **Branda SS, Gonzalez-Pastor JE, Ben-Yehuda S, Losick R, Kolter R.** 2001. Fruiting body formation by *Bacillus subtilis*. Proc. Natl. Acad. Sci. U. S. A. **98:**11621–11626. http://dx.doi.org/10.1073/pnas.191384198.
20. **Branda SS, Chu F, Kearns DB, Losick R, Kolter R.** 2006. A major protein component of the *Bacillus subtilis* biofilm matrix. Mol. Microbiol. **59:**1229–1238. http://dx.doi.org/10.1111/j.1365-2958.2005.05020.x.
21. **Romero D, Aguilar C, Losick R, Kolter R.** 2010. Amyloid fibers provide structural integrity to *Bacillus subtilis* biofilms. Proc. Natl. Acad. Sci. U. S. A. **107:**2230–2234. http://dx.doi.org/10.1073/pnas.0910560107.
22. **Ostrowski A, Mehert A, Prescott A, Kiley TB, Stanley-Wall NR.** 2011. YuaB functions synergistically with the exopolysaccharide and TasA amyloid fibers to allow biofilm formation by *Bacillus subtilis*. J. Bacteriol. **193:**4821–4831. http://dx.doi.org/10.1128/JB.00223-11.
23. **Kobayashi K, Iwano M.** 2012. BslA(YuaB) forms a hydrophobic layer on the surface of *Bacillus subtilis* biofilms. Mol. Microbiol. **85:**51–66. http://dx.doi.org/10.1111/j.1365-2958.2012.08094.x.
24. **Hobley L, Ostrowski A, Rao FV, Bromley KM, Porter M, Prescott AR, MacPhee CE, van Aalten DM, Stanley-Wall NR.** 2013. BslA is a self-assembling bacterial hydrophobin that coats the *Bacillus subtilis* biofilm. Proc. Natl. Acad. Sci. U. S. A. **110:**13600–13605. http://dx.doi.org/10.1073/pnas.1306390110.
25. **Stover AG, Driks A.** 1999. Secretion, localization, and antibacterial activity of TasA, a *Bacillus subtilis* spore-associated protein. J. Bacteriol. **181:**1664–1672.
26. **Stover AG, Driks A.** 1999. Control of synthesis and secretion of the *Bacillus subtilis* protein YqxM. J. Bacteriol. **181:**7065–7069.
27. **Terra R, Stanley-Wall NR, Cao G, Lazazzera BA.** 2012. Identification of *Bacillus subtilis* SipW as a bifunctional signal peptidase that controls surface-adhered biofilm formation. J. Bacteriol. **194:**2781–2790. http://dx.doi.org/10.1128/JB.06780-11.
28. **Romero D, Vlamakis H, Losick R, Kolter R.** 2011. An accessory protein required for anchoring and assembly of amyloid fibres in *B. subtilis* biofilms. Mol. Microbiol. **80:**1155–1168. http://dx.doi.org/10.1111/j.1365-2958.2011.07653.x.
29. **Chai L, Romero D, Kayatekin C, Akabayov B, Vlamakis H, Losick R, Kolter R.** 2013. Isolation, characterization, and aggregation of a structured bacterial matrix precursor. J. Biol. Chem. **288:**17559–17568. http://dx.doi.org/10.1074/jbc.M113.453605.
30. **Doan T, Marquis KA, Rudner DZ.** 2005. Subcellular localization of a sporulation membrane protein is achieved through a network of interactions along and across the septum. Mol. Microbiol. **55:**1767–1781. http://dx.doi.org/10.1111/j.1365-2958.2005.04501.x.
31. **Yasbin RE, Young FE.** 1974. Transduction in *Bacillus subtilis* by bacteriophage SPP1. J. Virol. **14:**1343–1348.
32. **Vlamakis H, Aguilar C, Losick R, Kolter R.** 2008. Control of cell fate by the formation of an architecturally complex bacterial community. Genes Dev. **22:**945–953. http://dx.doi.org/10.1101/gad.1645008.
33. **Szklarczyk R, Heringa J.** 2004. Tracking repeats using significance and transitivity. Bioinformatics **20**(Suppl 1):i311–i317. http://dx.doi.org/10.1093/bioinformatics/bth911.
34. **Liu C, Sawaya MR, Eisenberg D.** 2011. Beta-microglobulin forms three-

dimensional domain-swapped amyloid fibrils with disulfide linkages. Nat. Struct. Mol. Biol. **18:**49–55. http://dx.doi.org/10.1038/nsmb.1948.

35. **Kolodkin-Gal I, Romero D, Cao S, Clardy J, Kolter R, Losick R.** 2010. D-Amino acids trigger biofilm disassembly. Science **328:**627–629. http://dx.doi.org/10.1126/science.1188628.
36. **Leiman SA, May JM, Lebar MD, Kahne D, Kolter R, Losick R.** 2013. D-Amino acids indirectly inhibit biofilm formation in *Bacillus subtilis* by interfering with protein synthesis. J. Bacteriol. **195:**5391–5395. http://dx.doi.org/10.1128/JB.00975-13.
37. **Blanco LP, Evans ML, Smith DR, Badtke MP, Chapman MR.** 2012. Diversity, biogenesis and function of microbial amyloids. Trends Microbiol. **20:**66–73. http://dx.doi.org/10.1016/j.tim.2011.11.005.
38. **Robinson LS, Ashman EM, Hultgren SJ, Chapman MR.** 2006. Secretion of curli fibre subunits is mediated by the outer membrane-localized CsgG protein. Mol. Microbiol. **59:**870–881. http://dx.doi.org/10.1111/j.1365-2958.2005.04997.x.
39. **Taylor JD, Zhou Y, Salgado PS, Patwardhan A, McGuffie M, Pape T, Grabe G, Ashman E, Constable SC, Simpson PJ, Lee WC, Cota E, Chapman MR, Matthews SJ.** 2011. Atomic resolution insights into curli fiber biogenesis. Structure **19:**1307–1316. http://dx.doi.org/10.1016/j.str.2011.05.015.
40. **Dutton RJ, Boyd D, Berkmen M, Beckwith J.** 2008. Bacterial species exhibit diversity in their mechanisms and capacity for protein disulfide bond formation. Proc. Natl. Acad. Sci. U. S. A. **105:**11933–11938. http://dx.doi.org/10.1073/pnas.0804621105.
41. **Grana-Montes R, de Groot NS, Castillo V, Sancho J, Velazquez-Campoy A, Ventura S.** 2012. Contribution of disulfide bonds to stability, folding, and amyloid fibril formation: the PI3-SH3 domain case. Antioxid. Redox Signal. **16:**1–15. http://dx.doi.org/10.1089/ars.2011.3936.
42. **Kumar S, Ravi VK, Swaminathan R.** 2008. How do surfactants and DTT affect the size, dynamics, activity and growth of soluble lysozyme aggregates? Biochem. J. **415:**275–288. http://dx.doi.org/10.1042/BJ20071499.
43. **Sarkar N, Kumar M, Dubey VK.** 2011. Effect of sodium tetrathionate on amyloid fibril: insight into the role of disulfide bond in amyloid progression. Biochimie **93:**962–968. http://dx.doi.org/10.1016/j.biochi.2011.02.006.
44. **Sawyer EB, Claessen D, Haas M, Hurgobin B, Gras SL.** 2011. The assembly of individual chaplin peptides from *Streptomyces coelicolor* into functional amyloid fibrils. PLoS One **6:**e18839. http://dx.doi.org/10.1371/journal.pone.0018839.
45. **Branda SS, Gonzalez-Pastor JE, Dervyn E, Ehrlich SD, Losick R, Kolter R.** 2004. Genes involved in formation of structured multicellular communities by *Bacillus subtilis*. J. Bacteriol. **186:**3970–3979. http://dx.doi.org/10.1128/JB.186.12.3970-3979.2004.
46. **Chu F, Kearns DB, Branda SS, Kolter R, Losick R.** 2006. Targets of the master regulator of biofilm formation in *Bacillus subtilis*. Mol. Microbiol. **59:**1216–1228. http://dx.doi.org/10.1111/j.1365-2958.2005.05019.x.